ACS APPLIED MATERIALS & INTERFACES

Research Article

www.acsami.org

Vertically Aligned Ge Nanowires on Flexible Plastic Films Synthesized by (111)-Oriented Ge Seeded Vapor−Liquid−Solid Growth

Kaoru Toko,*[,†] Mitsuki Nakata,[†] Wipakorn Jevasuwan,[‡] Naoki Fukata,[‡] and Takashi Suemasu[†]

[†]Institute of Applied Physics, University of Tsukuba, Tsukuba, Ibaraki 305-8573, Japan

[‡]International Center for Materials Nanoarchitectonics, National Institute for Materials Science, Namiki, Tsukuba, Ibaraki 305-0044, Japan

ABSTRACT: Transfer-free fabrication of vertical Ge nanowires (NWs) on a plastic substrate is demonstrated using a vapor−liquid−solid (VLS) method. The crystal quality of Ge seed layers (50 nm thickness) prepared on plastic substrates strongly influenced the VLS growth morphology, i.e., the density, uniformity, and crystal quality of Ge NWs. The metal-induced layer exchange yielded a (111)-oriented Ge seed layer at 325 °C, which allowed for the VLS growth of vertically aligned Ge NWs. The Ge NW array had almost the same quality as that formed on a bulk Ge(111) substrate. Transmission electron microscopy demonstrated that the Ge NWs were defect-free single crystals. The present investigation paves the way for advanced electronic optical devices integrated on a low-cost flexible substrate.

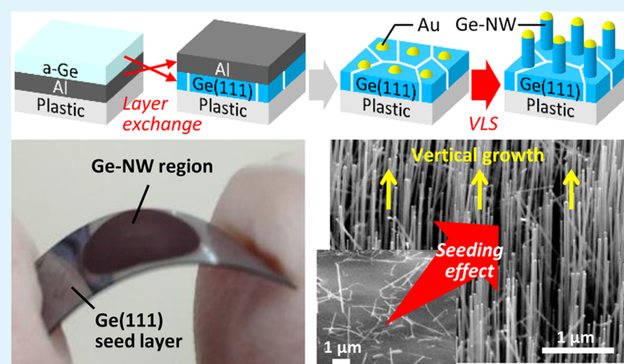

KEYWORDS: *germanium nanowires, flexible substrates, crystal orientation control, chemical vapor deposition, metal-induced crystallization*

1. INTRODUCTION

Ge nanowires (NWs) have been actively investigated for over a decade for fabricating high-performance transistors,[1] photodetectors,[2] and Li ion batteries.[3] To synthesize Ge NWs, researchers have developed many techniques, such as laser ablation[4] and vapor transport.[5] Chemical vapor deposition (CVD) via the metal-catalyzed vapor−liquid−solid (VLS) mechanism is one of the most popular synthesis methods.[6−16] 16 In the VLS method, Ge NWs grow in the ⟨111⟩ direction when the diameter of the metal catalysts is larger than approximately 10 nm.[8,9] Because the direction control of NWs is essential for producing NW devices,[17−20] (111)-oriented Si or Ge substrates have been used for growing vertically aligned NW arrays.[12−16]

However, the use of bulk substrates limits the application of NW devices. If aligned NWs are synthesized on amorphous insulators, such as SiO_2 or glass, NW devices can be fabricated in various devices, including man−machine interfaces, photovoltaics, and three-dimensional large-scale integrated circuits.[21−24] Using flexible plastic films as a substrate further expands the application of NW devices.[25−30] Transferring aligned NWs to SiO_2,[23] glass,[24] or plastic films[27−30] is a promising technique; however, there are difficulties keeping the process costs low and fabricating large-area devices, such as displays or solar cells. Some studies report directly grown Ge NWs on amorphous substrates, resulting in disordered NW structures because the growth occurred in random directions.[31,32]

To grow aligned Ge NWs on amorphous substrates, this study investigates a way using a (111)-oriented Ge seed layer formed by Al-induced crystallization (AIC). The concept is shown in Figure 1. AIC has been reported as a technique to

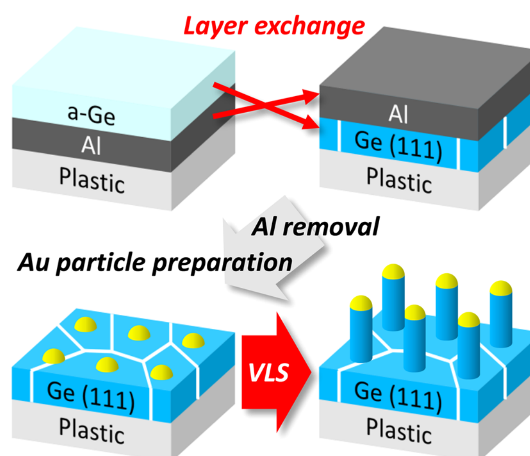

Figure 1. Concept of this study: how to grow vertically aligned Ge NWs on a flexible plastic substrate. A (111)-oriented Ge seed layer is formed by AIC via layer exchange, followed by VLS growth using CVD and Au particles.

Received: June 18, 2015
Accepted: July 31, 2015
Published: July 31, 2015

ACS Publications © 2015 American Chemical Society

DOI: 10.1021/acsami.5b05394
ACS Appl. Mater. Interfaces 2015, 7, 18120−18124

control the crystal orientation of Si on glass via the layer exchange between Si and Al.[33−35] The mechanism of layer exchange is understood as follows: First, Si atoms diffuse from metastable amorphous Si into Al during annealing. When the Si concentration in Al is supersaturated, Si nucleates. The continuous supply of Si atoms induces the lateral growth of Si crystals, which pushes Al to the upper layer. Eventually, Si forms the bottom layer while Al forms the upper layer. Using (111)-oriented AIC-Si as a seed layer, Cohin et al. achieved vertical GaAs NWs on a SiO_2 substrate.[36] Recently, we fabricated a highly (111)-oriented Ge layer on glass and even on plastic films at low temperatures (180−375 °C) by finding and optimizing the important growth parameters in AIC.[37−39] The AIC-Ge layer was useful as a seed layer for the molecular beam epitaxy of a high-quality Ge layer.[40] In the present paper, we investigate a transfer-free technique synthesizing aligned Ge NWs on flexible plastic films. Combining the VLS method with the orientation-controlled Ge seed layer formed by AIC, a vertically aligned, defect-free Ge NW array is demonstrated.

2. EXPERIMENTAL SECTION

The VLS growth of Ge NWs was performed using various substrates, as presented in Table 1. Sample A is a standard specimen with a Ge(111) substrate. Samples B−E have a flexible polyimide substrate (125 μm in thickness, Du Pont-Toray Co., Ltd.) with a heatproof temperature of 400 °C. The following depositions were carried out using a radio frequency magnetron sputtering (base pressure 3.0 × 10^{-4} Pa) with Ar plasma, where the deposition rates were 10 nm min^{-1} for SiO_2, 28 nm min^{-1} for Ge, and 31 nm min^{-1} for Al. The polyimide substrates were coated with 100 nm thick SiO_2 layers to avoid outgassing of the polyimide substrates in vacuum chambers. On the SiO_2 layers, we prepared amorphous Ge (a-Ge) at room temperature for sample C and polycrystalline Ge (poly-Ge) at 375 °C for sample D (50 nm thickness each). The grain size of the poly-Ge was a few tens of nanometers. For sample E, the AIC-Ge layer was prepared as follows: A 50 nm thick Al layer was prepared on the SiO_2 layer, and then exposed to air for 10 min to form a native AlO_x membrane as a diffusion-limiting layer,[37−39] followed by preparing a 50 nm thick a-Ge layer. Then the sample was annealed at 325 °C in N_2 for 100 h to induce layer exchange between Ge and Al. The Ge islands and Al layer, remaining in the top layer, are sequentially removed using H_2O_2 (50% H_2O_2) solution for 30 min and HF (1.5% HF) solution for 1 min.[40] Subsequently, Ge NWs were prepared for samples A−E as follows: All samples were cleaned using HF solution (1.5% HF), followed by preparing Au nanocolloid particles (40 nm in diameter) on the surfaces. Then CVD (base pressure 2.0 × 10^{-6} Pa) using 10 sccm GeH_4 (100%) was performed at 360 °C for 10 min, where the pressure was set at 8 Torr by mixing with N_2 gas.

Table 1. Samples Prepared in This Study

sample	substrate	process temperature for preparing the substrate
A	bulk Ge(111)	
B	SiO_2/plastic	rt
C	a-Ge/SiO_2/plastic	rt
D	poly-Ge/SiO_2/plastic	375 °C
E	AIC-Ge/SiO_2/plastic	325 °C

3. RESULTS AND DISCUSSION

The growth morphology of samples A−D was observed using scanning electron microscopy (SEM). Figure 2a shows the result of sample A, indicating that Ge NWs are densely formed and vertically aligned without tapering. The inset in Figure 2a suggests that each NW has a Au particle on its head. Thus, this VLS condition is appropriate for epitaxially growing Ge NWs in the ⟨111⟩ direction. In contrast, Figure 2b shows that sample B has remarkably few NWs. Besides, unreacted Au particles were observed on the SiO_2 surface. These may have occurred because it is difficult for Ge atoms to adhere to SiO_2 during CVD.[32,41] Figure 2c shows an SEM image of sample C, indicating that preparing an a-Ge seed layer significantly improves the density of NWs. Regarding sample D (Figure 2d), prepared with a poly-Ge seed layer, the density of Ge NWs is higher than that of sample C, and is almost the same as that of sample A. These results suggest that the nucleation frequency of Ge NWs depends on the crystal state of the seed layer: crystalline seed layers provide higher nucleation frequency than amorphous seed layers. Note that the Ge NWs of samples B−D, shown in Figure 2b−d, are disordered because their seed layers are not crystallographically oriented. Figure 2e schematically shows the VLS growth morphology of samples B−D. When the seed layer is amorphous or polycrystalline, Ge NWs do not grow, or grow in random directions. Therefore, a (111)-oriented seed layer is necessary to grow vertically aligned Ge NWs on a plastic substrate.

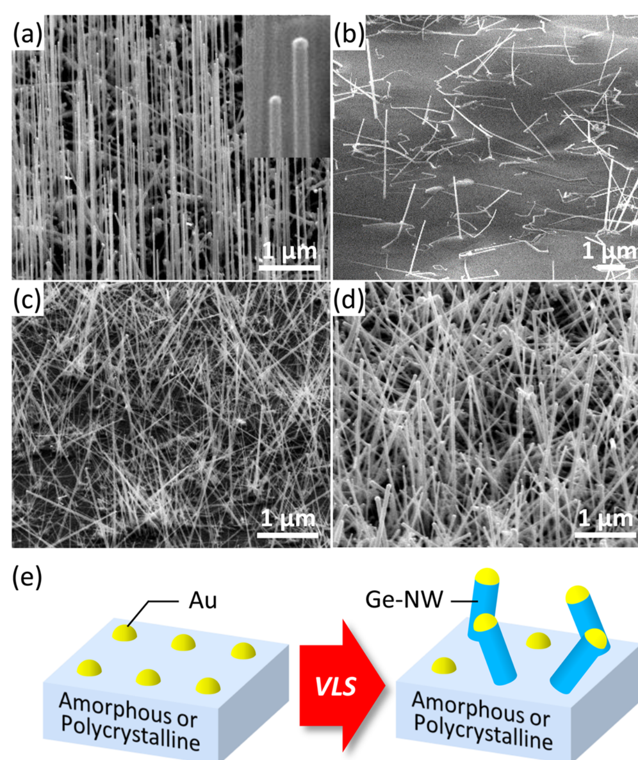

Figure 2. SEM images of samples (a) A, (b) B, (c) C, and (d) D, where the samples are 70° tilted. The inset in (a) shows a high-magnification SEM image of Ge NWs in sample A. (e) Schematic of the VLS growth of Ge NWs on amorphous or polycrystalline substrates.

The quality of the seed layer for sample E, formed by AIC, was characterized and is summarized in Figure 3. Figure 3a,b indicates that the Ge layer uniformly covers the plastic substrate, which is attributed to the complete layer exchange between Al and Ge layers. The Ge layer did not have cracks after being slightly bent as shown in Figure 3a. Figure 3b indicates that the Ge surface is a little rough, as a result of the initial shape of the Al layer.[34,37] The crystal orientation of Ge was evaluated using electron backscatter diffraction (EBSD) analysis. Figure 3c indicates that the Ge layer is highly (111)-

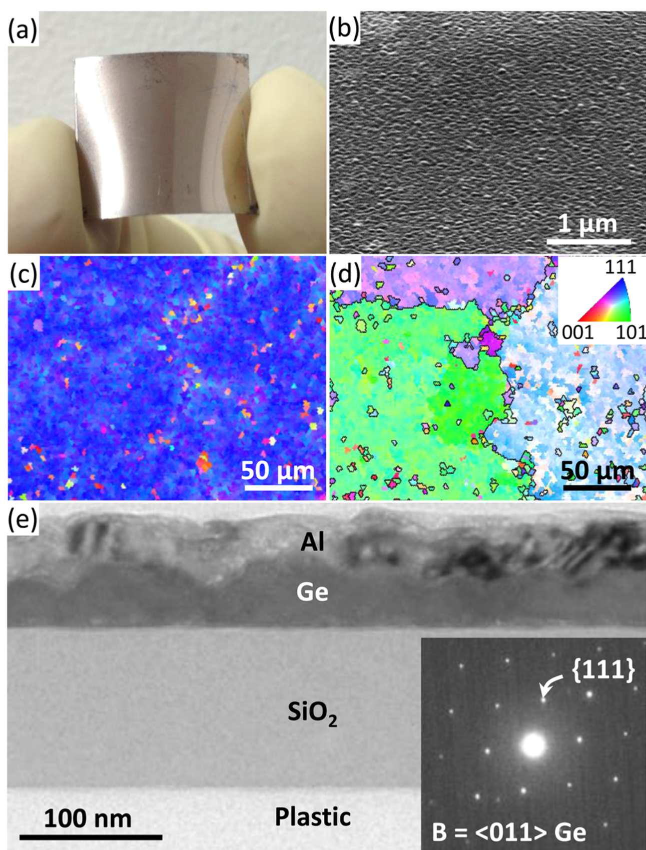

Figure 3. Characteristics of the Ge seed layer of sample E, formed by AIC. (a) Photograph of the sample. (b) SEM image of the sample, where the sample is 70° tilted. (c, d) EBSD images of the Ge layer, where the (c) ND and (d) TD maps correspond to the same region. (e) Cross-section TEM image, where the inset SAED pattern shows the Ge⟨011⟩ zone axis, taken of the sample.

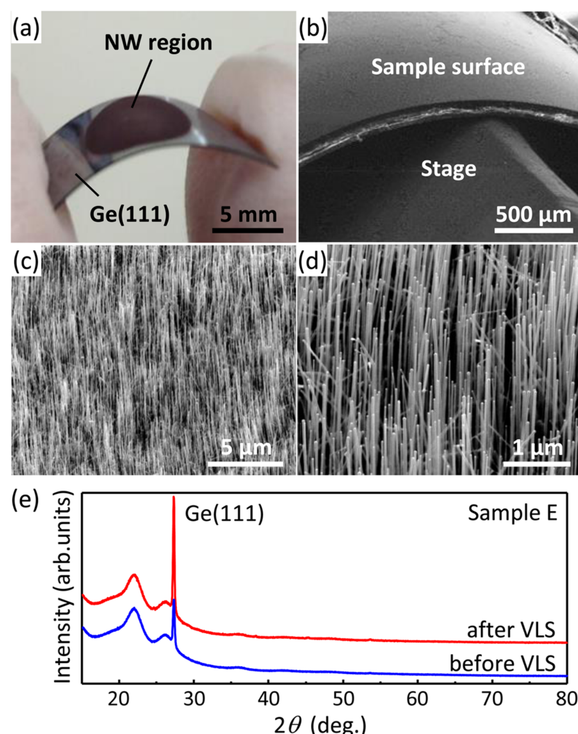

Figure 4. Characteristics of sample E after VLS growth. (a) Photograph of the sample. (b–d) SEM images of the sample with magnification of (b) 40×, (c) 5000×, and (d) 30000×, where the sample is 70° tilted. (e) XRD pattern of the sample. The XRD pattern of the sample before VLS growth is shown for comparison.

oriented in the normal direction (ND). The area fraction of the (111) orientation was calculated to be 96%. Such (111) orientation in AIC-Ge can be explained from the perspective of the appearance of the energetically stable plane.[37−39] As shown in Figure 3d, the crystal orientation in the transverse direction (TD) is random; however, the grain size is estimated to be larger than 100 μm. The cross-section structure was evaluated using transmission electron microscopy (TEM), where the sample was prepared by a conventional focused ion beam method. As representatively shown in Figure 3e, the Ge layer contained no obvious defects, such as stacking faults or disordered grain boundaries, in the region processed for TEM (6.4 μm in width). The selected area diffraction (SAED) pattern in Figure 3e indicates a single-crystal Ge layer, which is close to the (111) orientation in the direction normal to the substrate. From the SAED pattern, the lattice constant was calculated to be 0.566 nm, corresponding to relaxed Ge. Thus, we formed a high-quality (111)-oriented seed layer on a plastic substrate.

Sample E was characterized after the VLS growth and is summarized in Figure 4. Figure 4a shows that the sample has a circular red area corresponding to the area where the Au colloid was applied. This suggests the VLS growth of dense Ge NWs because NW structures cause the antireflection effect that is useful for fabricating high-efficiency optical devices.[17−19] As shown in Figure 4b, sample E was bent and attached to the sample stage of the scanning electron microscope. Figure 4c,d shows that the Ge NWs are densely formed, similar to those on a bulk Ge(111) substrate (Figure 2a) and vertically aligned even on the bent substrate. This is an advantage of aligned NW structures on a flexible substrate over those formed on a solid substrate.[25,30] The crystal orientation of Ge in sample E, before and after the VLS growth, was evaluated using a θ−2θ X-ray diffraction (XRD) measurement (spot size 10 mm). The resulting XRD patterns are shown in Figure 4e. Some broad peaks, especially at approximately 22° and 26°, correspond to the polyimide substrates. Sharp peaks at approximately 27.2° correspond to the (111) plane in Ge, while other peaks corresponding to Ge diffraction do not appear. The intensity of the (111) peak clearly increases after the VLS growth. These results indicate that the Ge NWs epitaxially grew from the (111)-oriented Ge seed layer.

The crystal quality of Ge NWs was compared among samples A−E using microprobe Raman scattering spectroscopy (spot size 1 μm, wavelength 532 nm). The representative Raman spectra are shown in Figure 5. For all samples, except sample B, which has few NWs, sharp peaks are observed at approximately 300 cm^{-1}, corresponding to the Ge−Ge vibration mode.[15] We obtained Raman spectra from several points in each sample and calculated the average value of the full width at half-maximum (fwhm) of the Ge−Ge peak. Note that the Ge−Ge peak of sample C is slightly flared at the bottom left because the a-Ge seed layer has a broad peak at approximately 277 cm^{-1}.[15] The effect of a-Ge was subtracted when the fwhm of sample C was calculated. The fwhm are shown in the inset. In the horizontal axis, the samples are arranged in the order of the crystal quality of the seed layer: a-Ge for sample C, poly-Ge for sample D , (111)-oriented Ge for sample E, and bulk Ge for sample A. Samples prepared with seed layers of higher quality provide

DOI: 10.1021/acsami.5b05394
ACS Appl. Mater. Interfaces 2015, 7, 18120−18124

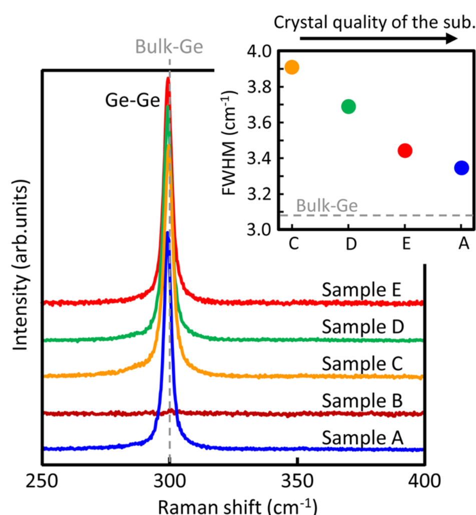

Figure 5. Raman spectra for samples A−E. The inset shows the fwhm values of the Ge−Ge peaks, where the samples are arranged in order of the crystal quality of the substrate in the horizontal axis. The peak position and fwhm of the Ge−Ge peak of a bulk Ge wafer are shown by dotted lines.

smaller fwhm values, indicating the higher quality of the resulting Ge NWs. This behavior can be explained as follows: Because the diameter of Au particles (approximately 40 nm) is larger than that of Ge nuclei (no more than 5 nm),[42] a few Ge nuclei may occur on the interface between a Au particle and a seed layer at the initial stage of VLS growth. When the seed layer is single crystalline or large grained, the initial Ge nuclei, epitaxially growing on a shared crystal, merge without forming defects. In contrast, when the seed layer is amorphous or small grained, the initial Ge nuclei differ from one another in the crystal orientations, and thus form defects as a result of their collisions. Therefore, the larger fwhm values for samples prepared with seed layers of lower quality are likely attributed to the defects on the bottom of NWs. Note that the fwhm of sample E is 3.41 cm^{-1}, close to that of sample A (3.32 cm^{-1}). This result indicates that the crystal quality of the Ge NWs on the plastic substrate approaches that on the bulk Ge substrate.

The detailed crystal structure of the Ge NWs in sample E was observed using TEM. The representative results are shown in Figure 6. Figure 6a shows that a Au catalyst, which activated the VLS growth, is present on the NW head. The NWs were not tapered and were approximately 40 nm in diameter, which was equal to the initial diameter of Au nanocolloid particles. Figure 6b and the inset lattice image indicate that the Ge NW has a fringe contrast corresponding to the {111} planes. This is evidence of the growth in the ⟨111⟩ direction. We observed several Ge NWs and found that they were single crystalline and had no defects, including dislocations or stacking faults in the entire region, as representatively shown in Figure 6. Thus, the TEM observation demonstrated defect-free single-crystal Ge NWs on a flexible plastic substrate.

4. CONCLUSION

We investigated a transfer-free technique for fabricating Ge NWs on a flexible plastic film using a VLS method. Although it was difficult to grow Ge NWs directly on a plastic substrate, preparing a-Ge or poly-Ge seed layers facilitated the NW growth. However, the resulting NW array was inhomogeneous because of the growth in random directions. We therefore formed a (111)-oriented Ge seed layer using AIC with layer exchange, which allowed for the direct synthesis of vertically aligned Ge NWs. TEM observation demonstrated that the Ge NWs were defect-free single crystals. Thus, we realized a Ge NW array on a plastic film, which had almost the same quality as that on a bulk Ge substrate. This achievement opens up the possibility for developing next-generation flexible devices that are simultaneously high performing and inexpensive.

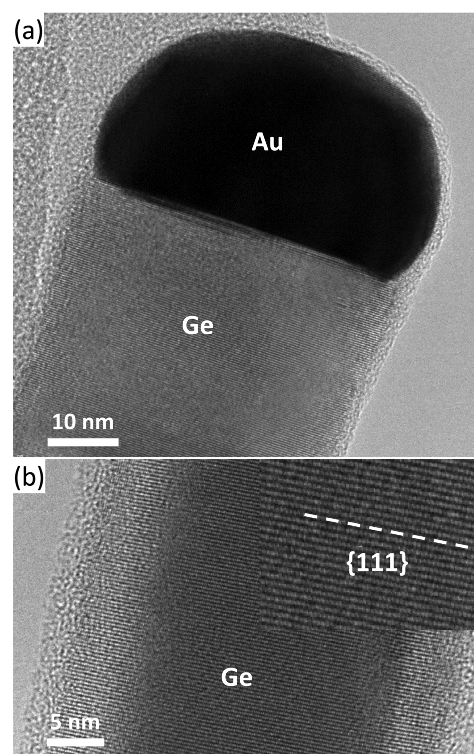

Figure 6. TEM images of the (a) head and (b) bottom of a Ge NW in sample E. The inset is a lattice image of the Ge NW showing {111} planes.

■ AUTHOR INFORMATION

Corresponding Author

*E-mail: toko@bk.tsukuba.ac.jp.

Notes

The authors declare no competing financial interest.

■ ACKNOWLEDGMENTS

This work was financially supported by the Japan Society for the Promotion of Science (JSPS) KAKENHI (Grants 26709019 and 26600083) and the JGC-S Scholarship Foundation. Some experiments were conducted at the International Center for Young Scientists at the National Institute for Materials Science (NIMS).

■ REFERENCES

(1) Xiang, J.; Lu, W.; Hu, Y.; Wu, Y.; Yan, H.; Lieber, C. M. Ge/Si Nanowire Heterostructures as High-Performance Field-Effect Transistors. *Nature* **2006**, *441*, 489−493.

(2) Kim, C.-J.; Lee, H.-S.; Cho, Y.-J.; Kang, K.; Jo, M.-H. Diameter-Dependent Internal Gain in Ohmic Ge Nanowire Photodetectors. *Nano Lett.* **2010**, *10*, 2043−2048.

(3) Wang, J.; Du, N.; Zhang, H.; Yu, J.; Yang, D. Cu−Ge Core−shell Nanowire Arrays as Three-Dimensional Electrodes for High-Rate

Capability Lithium-Ion Batteries. *J. Mater. Chem.* **2012**, *22*, 1511−1515.

(4) Lauhon, L. J.; Gudiksen, M. S.; Wang, D.; Lieber, C. M. Epitaxial Core-Shell and Core-Multishell Nanowire Heterostructures. *Nature* **2002**, *420*, 57−61.

(5) Wu, Y.; Yang, P. Germanium Nanowire Growth via Simple Vapor Transport. *Chem. Mater.* **2000**, *12*, 605−607.

(6) O'Regan, C.; Biswas, S.; Petkov, N.; Holmes, J. D. Recent Advances in the Growth of Germanium Nanowires: Synthesis, Growth Dynamics and Morphology Control. *J. Mater. Chem. C* **2014**, *2*, 14−33.

(7) Adhikari, H.; Marshall, A. F.; Goldthorpe, I. A.; Chidsey, C. E. D.; McIntyre, P. C. Metastability of Au-Ge Liquid Nanocatalysts: Ge Vapor-Liquid-Solid Nanowire Growth Far below the Bulk Eutectic Temperature. *ACS Nano* **2007**, *1*, 415−422.

(8) Dayeh, S. A.; Picraux, S. T. Direct Observation of Nanoscale Size Effects in Ge Semiconductor Nanowire Growth. *Nano Lett.* **2010**, *10*, 4032−4039.

(9) Adhikari, H.; Marshall, A. F.; Chidsey, C. E. D.; McIntyre, P. C. Germanium Nanowire Epitaxy: Shape and Orientation Control. *Nano Lett.* **2006**, *6*, 318−323.

(10) Kodambaka, S.; Tersoff, J.; Reuter, M. C.; Ross, F. M. Germanium Nanowire Growth below the Eutectic Temperature. *Science* **2007**, *316*, 729−732.

(11) Woodruff, J. H.; Ratchford, J. B.; Goldthorpe, I. A.; McIntyre, P. C.; Chidsey, C. E. D. Vertically Oriented Germanium Nanowires Grown from Gold Colloids on Silicon Substrates and Subsequent Gold Removal. *Nano Lett.* **2007**, *7*, 1637−1642.

(12) Sierra-Sastre, Y.; Choi, S.; Picraux, S. T.; Batt, C. A. Vertical Growth of Ge Nanowires from Biotemplated Au Nanoparticle Catalysts. *J. Am. Chem. Soc.* **2008**, *130*, 10488−10489.

(13) Koto, M.; Marshall, A. F.; Goldthorpe, I. A.; McIntyre, P. C. Gold-Catalyzed Vapor-Liquid-Solid Germanium-Nanowire Nucleation on Porous Silicon. *Small* **2010**, *6*, 1032−1037.

(14) Connell, J. G.; Al Balushi, Z. Y.; Sohn, K.; Huang, J.; Lauhon, L. J. Growth of Ge Nanowires from Au-Cu Alloy Nanoparticle Catalysts Synthesized from Aqueous Solution. *J. Phys. Chem. Lett.* **2010**, *1*, 3360−3365.

(15) Fukata, N.; Sato, K.; Mitome, M.; Bando, Y.; Sekiguchi, T.; Kirkham, M.; Hong, J. I.; Wang, Z. L.; Snyder, R. L. Doping and Raman Characterization of Boron and Phosphorus Atoms in Germanium Nanowires. *ACS Nano* **2010**, *4*, 3807−3816.

(16) Fukata, N.; Mitome, M.; Sekiguchi, T.; Bando, Y.; Kirkham, M.; Hong, J. I.; Wang, Z. L.; Snyder, R. L. Characterization of Impurity Doping and Stress in Si/Ge and Ge/Si Core-Shell Nanowires. *ACS Nano* **2012**, *6*, 8887−8895.

(17) Li, Y.; Clady, R.; Park, J.; Thombare, S. V.; Schmidt, T. W.; Brongersma, M. L.; McIntyre, P. C. Ultrafast Electron and Phonon Response of Oriented and Diameter-Controlled Germanium Nanowire Arrays. *Nano Lett.* **2014**, *14*, 3427−3431.

(18) Polyakov, B.; Daly, B.; Prikulis, J.; Lisauskas, V.; Vengalis, B.; Morris, M. a.; Holmes, J. D.; Erts, D. High-Density Arrays of Germanium Nanowire Photoresistors. *Adv. Mater.* **2006**, *18*, 1812−1816.

(19) Solanki, A.; Crozier, K. Vertical Germanium Nanowires as Spectrally-Selective Absorbers across the Visible-to-Infrared. *Appl. Phys. Lett.* **2014**, *105*, 191115.

(20) Tomioka, K.; Yoshimura, M.; Fukui, T. A III−V Nanowire Channel on Silicon for High-Performance Vertical Transistors. *Nature* **2012**, *488*, 189−192.

(21) Weng, W. Y.; Chang, S. J.; Hsu, C. L.; Hsueh, T. J. A ZnO-Nanowire Phototransistor Prepared on Glass Substrates. *ACS Appl. Mater. Interfaces* **2011**, *3*, 162−166.

(22) Schmitt, S. W.; Schechtel, F.; Amkreutz, D.; Bashouti, M.; Srivastava, S. K.; Hoffmann, B.; Dieker, C.; Spiecker, E.; Rech, B.; Christiansen, S. H. Nanowire Arrays in Multicrystalline Silicon Thin Films on Glass: A Promising Material for Research and Applications in Nanotechnology. *Nano Lett.* **2012**, *12*, 4050−4054.

(23) Tang, J.; Wang, C. Y.; Xiu, F.; Lang, M.; Chu, L. W.; Tsai, C. J.; Chueh, Y. L.; Chen, L. J.; Wang, K. L. Oxide-Confined Formation of Germanium Nanowire Heterostructures for High-Performance Transistors. *ACS Nano* **2011**, *5*, 6008−6015.

(24) Huang, J. S.; Hsiao, C. Y.; Syu, S. J.; Chao, J. J.; Lin, C. F. Well-Aligned Single-Crystalline Silicon Nanowire Hybrid Solar Cells on Glass. *Sol. Energy Mater. Sol. Cells* **2009**, *93*, 621−624.

(25) Liu, Z.; Xu, J.; Chen, D.; Shen, G. Flexible Electronics Based on Inorganic Nanowires. *Chem. Soc. Rev.* **2015**, *44*, 161−192.

(26) Liu, X.; Long, Y. Z.; Liao, L.; Duan, X.; Fan, Z. Large-Scale Integration of Semiconductor Nanowires for High-Performance Flexible Electronics. *ACS Nano* **2012**, *6*, 1888−1900.

(27) McAlpine, M. C.; Ahmad, H.; Wang, D.; Heath, J. R. Highly Ordered Nanowire Arrays on Plastic Substrates for Ultrasensitive Flexible Chemical Sensors. *Nat. Mater.* **2007**, *6*, 379−384.

(28) Timko, B. P.; Cohen-Karni, T.; Yu, G.; Qing, Q.; Tian, B.; Lieber, C. M. Electrical Recording from Hearts with Flexible Nanowire Device Arrays. *Nano Lett.* **2009**, *9*, 914−918.

(29) Lee, M.; Jeon, Y.; Moon, T.; Kim, S. Top-down Fabrication of Fully CMOS-Compatible Silicon Nanowire Arrays and Their Integration into CMOS Inverters on Plastic. *ACS Nano* **2011**, *5*, 2629−2636.

(30) Weisse, J. M.; Lee, C. H.; Kim, D. R.; Zheng, X. Fabrication of Flexible and Vertical Silicon Nanowire Electronics. *Nano Lett.* **2012**, *12*, 3339−3343.

(31) Wang, D.; Dai, H. Low-Temperature Synthesis of Single-Crystal Germanium Nanowires by Chemical Vapor Deposition. *Angew. Chem.* **2002**, *114*, 4977−4980.

(32) Sun, X.; Calebotta, G.; Yu, B.; Selvaduray, G.; Meyyappan, M. Synthesis of Germanium Nanowires on Insulator Catalyzed by Indium or Antimony. *J. Vac. Sci. Technol., B: Microelectron. Nanometer Struct.* **2007**, *25*, 415−420.

(33) Kurosawa, M.; Kawabata, N.; Sadoh, T.; Miyao, M. Orientation-Controlled Si Thin Films on Insulating Substrates by Al-Induced Crystallization Combined with Interfacial-Oxide Layer Modulation. *Appl. Phys. Lett.* **2009**, *95*, 132103.

(34) Wang, Z.; Gu, L.; Jeurgens, L. P. H.; Phillipp, F.; Mittemeijer, E. J. Real-Time Visualization of Convective Transportation of Solid Materials at Nanoscale. *Nano Lett.* **2012**, *12*, 6126−6132.

(35) Toko, K.; Numata, R.; Saitoh, N.; Yoshizawa, N.; Usami, N.; Suemasu, T. Selective Formation of Large-Grained, (100)- or (111)-Oriented Si on Glass by Al-Induced Layer Exchange. *J. Appl. Phys.* **2014**, *115*, 094301.

(36) Cohin, Y.; Mauguin, O.; Largeau, L.; Patriarche, G.; Glas, F.; Søndergård, E.; Harmand, J.-C. Growth of Vertical GaAs Nanowires on an Amorphous Substrate via a Fiber-Textured Si Platform. *Nano Lett.* **2013**, *13*, 2743−2747.

(37) Toko, K.; Kurosawa, M.; Saitoh, N.; Yoshizawa, N.; Usami, N.; Miyao, M.; Suemasu, T. Highly (111)-Oriented Ge Thin Films on Insulators Formed by Al-Induced Crystallization. *Appl. Phys. Lett.* **2012**, *101*, 072106.

(38) Toko, K.; Numata, R.; Oya, N.; Fukata, N.; Usami, N.; Suemasu, T. Low-Temperature (180 °C) Formation of Large-Grained Ge (111) Thin Film on Insulator Using Accelerated Metal-Induced Crystallization. *Appl. Phys. Lett.* **2014**, *104*, 022106.

(39) Oya, N.; Toko, K.; Saitoh, N.; Yoshizawa, N.; Suemasu, T. Direct Synthesis of Highly Textured Ge on Flexible Polyimide Films by Metal-Induced Crystallization. *Appl. Phys. Lett.* **2014**, *104*, 262107.

(40) Toko, K.; Nakazawa, K.; Saitoh, N.; Yoshizawa, N.; Suemasu, T. Improved Surface Quality of the Metal-Induced Crystallized Ge Seed Layer and Its Influence on Subsequent Epitaxy. *Cryst. Growth Des.* **2015**, *15*, 1535−1539.

(41) Tada, M.; Park, J.-H.; Kuzum, D.; Thareja, G.; Jain, J. R.; Nishi, Y.; Saraswat, K. C. Low Temperature Germanium Growth on Silicon Oxide Using Boron Seed Layer and In Situ Dopant Activation. *J. Electrochem. Soc.* **2010**, *157*, H371−H376.

(42) Edelman, F.; Komem, Y.; Bendayan, M.; Beserman, R. Initial Crystallization Stage of Amorphous Germanium Films. *J. Appl. Phys.* **1992**, *72*, 5153−5157.